Impact of crowding on the diversity of expanding populations

Carl F. Schreck[a,b,*], Diana Fusco[a,b,c,*], Yuya Karita[d,*], Stephen Martis[a], Jona Kayser[a,b], Marie-Cécilia Duvernoy[a,b], Oskar Hallatschek[a,b,1]

[*]C.F.S., D.F., and Y.K. contributed equally to this work.
[a]Department of Physics, University of California, 94709 CA, Berkeley
[b]Department of Integrative Biology, University of California, 94709 CA, Berkeley
[c]Department of Physics, University of Cambridge, CB3 0HE, Cambridge, United Kingdom
[d]Graduate Program in Biophysics, University of California, 94709 CA, Berkeley

E-mail: [1]ohallats@berkeley.edu

Abstract. Crowding effects are key to the self-organization of densely packed cellular assemblies, such as biofilms, solid tumors, and developing tissues. When cells grow and divide they push each other apart, remodeling the structure and extent of the populations range. It has recently been shown that crowding effects also couple the evolutionary fate of neighboring cells, thereby weakening the strength of natural selection. However, the impact of crowding on neutral processes remains unclear. Here, we quantify the genetic diversity of expanding microbial colonies and uncover signatures of crowding in the site frequency spectrum. By combining fluctuation tests, cell-based simulations, and lineage tracing in a novel microfluidic incubator, we find that the majority of mutations arise behind the expanding frontier, giving rise to clones that are mechanically "pushed out" of the growing region by the proliferating cells in front. These excluded-volume interactions result in a clone size distribution that solely depends on *where* the mutation first arose relative to the front and is characterized by a simple power-law for sizes below a critical threshold. Our model and simulations predict that the distribution only depends on a single parameter, the characteristic growth layer thickness, and hence allows estimation of the mutation rate in a variety of crowded cellular populations. Combined with previous studies on high-frequency mutations, our finding provides a unified picture of the genetic diversity in expanding populations over the whole frequency range and suggests a practical method to assess growth dynamics by sequencing populations across scales.

Keywords: Genetic variation, Clone size distribution, Biofilms, Intra-tumor heterogeneity

C.F.S., D.F., Y.K., S.M. and O.H. designed and developed the study. D.F., Y.K. and S.M. conducted the fluctuation experiments. J.K. engineered the yeast strain. Y.K. and M.-C.D. conducted the microfluidic experiments. C.F.S. developed the cell-based simulations. C.F.S., S.M., and D.F. derived the mathematical model. C.F.S., D.F., Y.K., S.M., and O.H. wrote the manuscript.

1. Introduction

Environmental factors often structure the spatial organization of growing cellular populations, such as microbial biofilms [1], developing embryos and differentiating tissues [2], as well as solid tumors [3, 4, 5, 6]. Advances in lineage tracing techniques are progressively revealing that in many of these cases growth is non-uniform across the population, as it strongly depends on the mechanical and biochemical cues experienced by each cell [7, 8, 9, 10, 11, 4, 12, 13, 14, 5]. Non-uniform growth can favor individuals based on their spatial locations rather than their fitness [15, 16, 17, 18, 6] and as such can dramatically impact the evolutionary fate of the population.

The interplay between evolution and growth has been extensively investigated in the context of range expansions, in which populations grow by invading surrounding virgin territory [19, 20, 21, 22, 23, 24, 25]. In cellular range expansions, growth is often limited to a thin layer of cells at the expanding front of the population (the *growth layer*) due to processes like nutrient depletion, waste accumulation, mechanical pressure, or quorum sensing in the bulk [26, 27, 28, 29, 30, 31, 32]. Recent studies have revealed that this growth constraint generates an excess of high-frequency mutations in microbial colonies [33] and colorectal cancer xenografts [6]. Remarkably, the size distribution of these large clones is exclusively determined by the surface growth properties of the population through a phenomenon called allele surfing [19, 34].

The distribution of low-frequency mutations, however, remains an open question. Assuming a mutation rate of 10^{-3} mutation/genome/generation (typical of microbes) and a population size of $10^8 \sim 10^9$ cells, a total of $10^5 \sim 10^6$ mutations are generated during population growth. Yet, experimentally only approximately 0.001 % of these mutations have been captured by population sequencing in the case of bacterial colonies and tumors [33, 35, 36, 37]. This suggests that low-frequency mutations constitute the majority of genetic diversity in the population, but since their frequency is often below the detection limit of population sequencing, they go undetected. As a single mutant can be sufficient to drive drug resistance [15], its quantification is imperative to better understand the emergence of resistant cells after drug treatment. While several groups have recently revealed the dynamics of small clones by multicolor lineage tracing in solid tumors [5, 6, 12], a quantitative understanding of the dynamics of low-frequency mutations is still lacking. Here, we address this gap by investigating the dynamics of low-frequency mutations utilizing an expanding microbial colony as a model system.

To probe the low-frequency end of the mutational spectrum, we adapted the classic Luria-Delbrück fluctuation test, normally used to infer mutation rates in well-mixed populations [38], to microbial colonies. We find that the vast majority of mutations occurring during growth are present at very low frequencies and characterized by a clone size distribution that decays faster than the one observed at high frequency [33], with a crossover frequency determined by the width of the growth layer. Using cell-based computer simulations that explicitly mimic mechanical repulsive forces between proliferating cells in crowded colonies, we track the dynamics of individual clones. The

simulations suggest that small clones stem from mutations that occur just behind the very front of the expanding edge. As the front expands, the cells proliferating at the very front continuously push back those behind, which are destined to eventually fall out of the growth layer and stop dividing. The resulting clone size distribution reflects the crowding dynamics within the growth layer. To test our analytical predictions in a cellular system, we designed a microfluidic device for continuous cell culture, which we name the population machine inspired by the so-called mother machine [39]. Combined with a newly engineered color-switching *S. cerevisiae* strain, based on technology previously used in studies [33, 40], the population machine enables visual clonal lineage tracking in confined populations for up to ten generations. The population machine, which we considered to be a growth layer with a pinned front, is a model of growth layer dynamics in freely-expanding populations.

2. Results

2.1. Fluctuation test in bacterial colonies

To assess the clone size distributions of small clones ($< 10^4$ cells) in *E. coli* colonies grown from single cells to $\approx 10^9$ cells, we adapted the Luria-Delbrück fluctuation test [38], routinely used to determine spontaneous rates of resistant mutations in well-mixed populations [41, 42, 43, 44, 45], to structured populations like colonies. Colonies were grown on rich non-selective media, scooped up completely after two days of growth, resuspended, and then plated on selective plates containing nalidixic acid (see Methods). After overnight growth, the selective plates were imaged and the number of resistant colony forming units (CFUs) were counted (Methods).

The resulting distribution exhibits a decay that resembles the classic Luria-Delbrück distribution typical of well-mixed populations (dashed blue line in Fig. 1), in contrast to the distribution of large mutant clones (more than 10^5 cells) previously observed in similar colonies of the same strain via population sequencing (dashed red line) [33]. Indeed, comparison in the clone size distribution pre-factors between colonies and well-mixed populations from sequencing data had previously hinted to the necessary presence of a different distribution regime at very low frequencies [33]. In the following, we investigate the physical origin of these low-frequency clones and characterize their statistics.

2.2. Mechanical simulations

The mechanical process underlying colony expansion has been recently found to have important evolutionary consequences for the strength of genetic drift [26] and natural selection [31, 32]. To gain an intuition into whether mechanical forces can generate the distribution of small clones we observe, we employed 2D mechanical simulations where individually-modeled cells proliferate and repel each other upon contact (see Methods)[31, 47]. We introduced an explicit growth layer of finite width λ within which

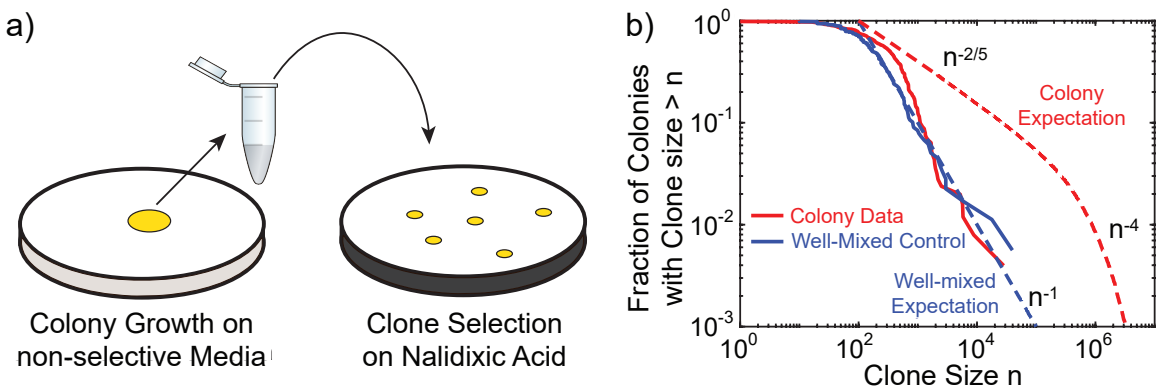

Figure 1. Fluctuation test in bacterial colonies reveals a distinct clone size distribution at low frequencies. (a) Fluctuation test on 234 *E. coli* colonies that were grown for two days, completely harvested and then plated on nalidixic acid. The size of clones corresponding to resistant mutations was determined by counting the number of CFUs on selective plates. (b) Fraction of the sampled colonies carrying at least n resistant mutants (red solid line) in comparison with the well-mixed control (blue solid lines). The blue dashed line corresponds to the classic Luria-Delbrück distribution for well-mixed populations (n^{-1}) [46], while the red dashed line corresponds to large clones (bubbles and sectors) found in colonies ($n^{-2/5}$ and n^{-4}) [33].

cells grow exponentially at a constant rate (Fig 2a). Beyond the growth layer, cells are considered to be in the *bulk* and stop growing. We represented proliferation via budding in order to make a connection to our microfluidic budding yeast experiments with budding yeast described later (Fig. 3). In fact, clone size distributions are not sensitive to cell shape or the details of division type (Fig. S6).

The clone size distribution obtained from the simulations shows a transition between two regimes (Fig. 2b): very small clones ($n \lessapprox \lambda$, see Fig. S1) appear to follow n^{-1}, while larger clones follow a shallower power-law in quantitative agreement with the allele surfing prediction. We find that the shallower power-law consists of mutations that arose at the very front of the growth layer and surfed the edge for some time (red clone in Fig. 2a and red line in Fig. 2b). By contrast, small clones stem from mutations that occur behind the front (blue clone in Fig. 2a and blue line in Fig. 2b). These clones never surf on the expanding edge but grow while inside the growth layer until they are pushed out by the proliferating cells in front.

When looking at individual non-surfing clones, defined as those arising more than a cell diameter from the front, we find a reproducible relationship between the final clone size and the position where the corresponding mutation first arose (Fig. 2c).

Crowding model of non-surfing clones

To uncover the physical mechanisms underlying non-surfing clones, we developed a mathematical model that describes what we observe in the simulations. As in the simulations, we assumed that the growth rate is constant within a distance λ of the

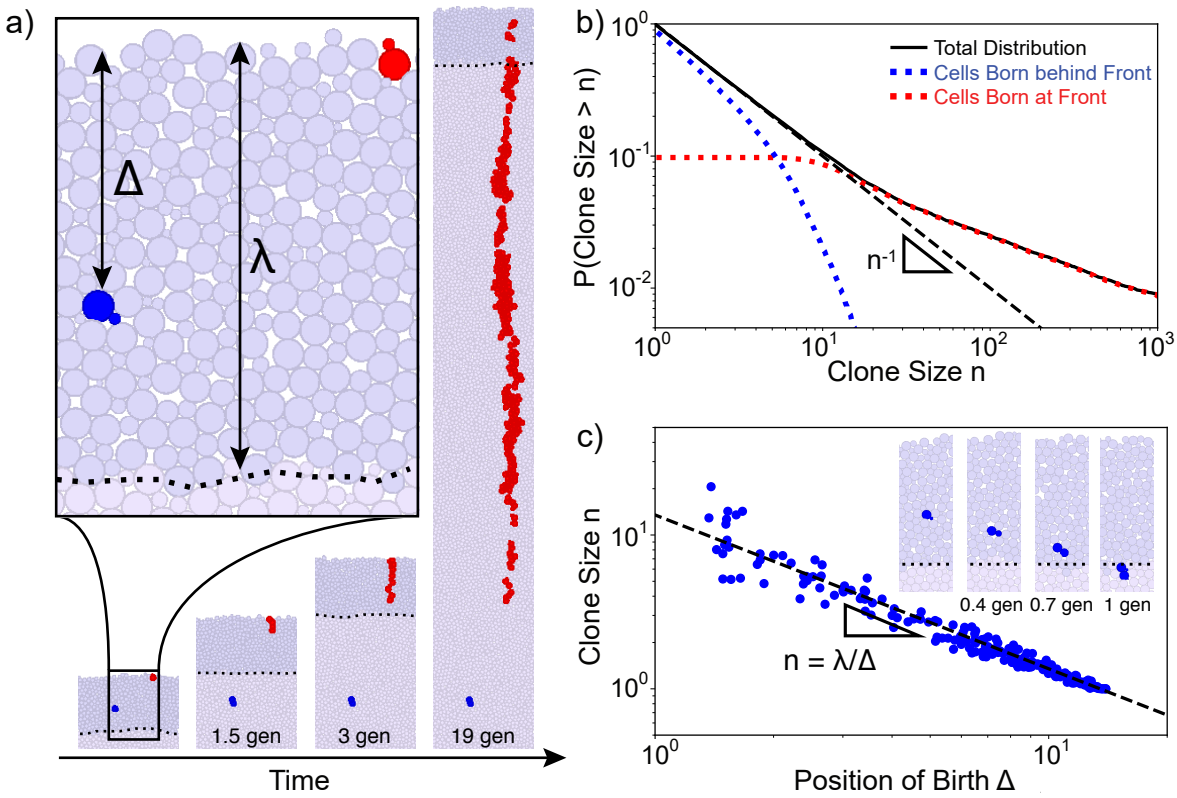

Figure 2. Cell-based simulations show different behaviors between surfing and non-surfing clones. (a) Illustration of the mechanical simulations. Cells lying in the growth layer, defined as the region within a distance $\Delta < \lambda$ from the front (dark purple region with dashed line showing back of growth layer), replicate exponentially. In this image, $\lambda = 14$ cell diameters (about 50 μm). As growth proceeds, the front moves at a constant speed and cells behind the front are continuously pushed out of the growth layer by replicating cells in front due to excluded-volume interactions. Mutations can either occur at the very front (red cells) generating a surfing clone, or behind the front (blue cells) generating non-surfing clones that are quickly washed out of the growth layer. Clonal dynamics are shown for the first 20 generations of cellular growth. (b) The full clone distribution (solid black line) can be subdivided in the size distribution of surfing clones (red dotted line), which dominate the high-frequency tail of the distribution, and non-surfing clones (blue dotted line), that dominates the low-frequency behavior. The dashed black line shows the n^{-1} prediction. (c) Scatter-plot identifying for each clone (blue dot) the distance from the front at which the mutation first arose and the final clone size upon exiting the growth layer. Surfing clones are by definition clones that arose within 1 cell distance from the front. Non-surfing clones appear to satisfy the predicted relationship $n = \lambda/\Delta$ (dashed black line). The inset shows the dynamics of the blue clone a short time (< 1 generation) after birth in the reference frame of the front. This clone is born at distance $\Delta = 7$ cells from the front and grows to a size of $n = 2$.

expanding front and zero otherwise. We analyzed clones in a reference frame that is co-moving with the expanding front, so that rather than accumulating at the edge of the colony, cells are washed out towards the colony bulk (Fig. 2c inset). A mutant of infinitesimal size δn_0 born at a distance Δ from the front will grow until it is pushed out of the growth layer by excluded volume effects from the cells proliferating in front. This happens when the cells in front have grown to size λ to fill the growth layer. Because growth is constant within the growth layer, the mutant will grow by the same relative amount as the layers of cells in front, reaching a final size $\delta n = \frac{\lambda}{\Delta}\delta n_0$. By extending this infinitesimal relation to mutant clones with $n_0 = 1$ cell at the onset of mutation, we have the prediction (see SI Section 1 for finite-size analysis)

$$n \approx \frac{\lambda}{\Delta}, \tag{1}$$

in agreement with the cell-based mechanical simulations (Fig. 2b).

Equation 1 translates into a prediction for the clone size distribution when combined with the probability of observing a mutation at distance Δ. If we assume that the mutation rate is proportional to the growth rate, the probability that a mutation will occur at $\Delta < \lambda$ is $P(\Delta) = \lambda^{-1}$. Then, the probability of observing a clone of size n is

$$P(n) = P(\Delta) \times |d\Delta/dn| = \lambda^{-1} \times \lambda/n^2 = n^{-2}, \tag{2}$$

corresponding to a cumulative clone size distribution of $P(\text{Clone size} > n) = 1/n$. This result is based on the assumption that the mutant clone size (n) is smaller than the growth layer depth (λ). We show in SI Section 1 that $P(n) = n^{-2}$ holds very well up to $n = \lambda$, corresponding to mutants born exactly $\Delta = 1$ cell diameter behind the front. Additionally, in SI Section 2 we discuss that our argument also holds in the case of non-uniform growth rate inside the growth layer.

Clone tracking experiments in microfluidics

The mathematical argument presented above suggests that the only factor that matters to generate small clones in a spatially expanding population is the crowding dynamics in the growth layer. Therefore, to reproduce the predicted clone size distribution in an experiment, it should be sufficient to track the dynamics at the growth layer. To test this hypothesis in a cellular system, we designed an *in vitro* growth layer using a microfluidic chamber that allows to visually track growth and spatial dynamics of color-switching *S. cerevisiae* cells for 2-4 days (Fig. 3a, b and Methods). The design of the device was inspired by previous studies [48, 49, 50, 51, 39]. In the chamber, all cells grow at the same rate (Fig. S4) and are continuously pushed out as the cells in front proliferate and fill the space, capturing the mechanical interactions between cells at the growing edge of a colony in its co-moving frame.

To investigate the dynamics of clones from a single mutational event, we conducted lineage tracking experiments with an engineered yeast strain that stochastically switches from one fluorescent color to another (Methods and Fig. S3). Since the switch can occur only at cell division, is heritable and does not measurably change the growth

rate (Fig. S5), it should effectively behave like a neutral mutation, whose position and growth can be visually tracked with fluorescent microscopy.

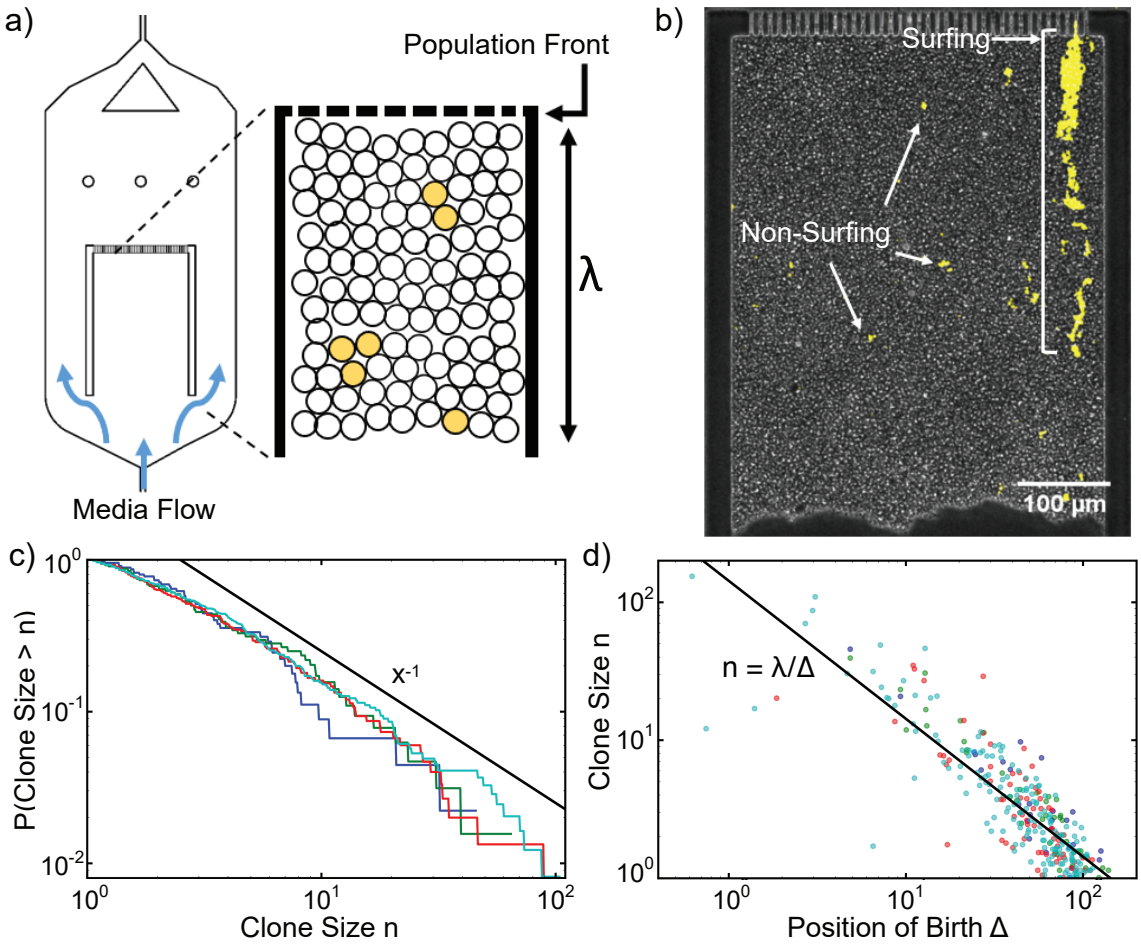

Figure 3. Our novel microfluidic incubator allows to track the front dynamic over several generations. (a,b) A schematic image and snapshot of the microfluidic experiments. A population of yeast cells in the chamber models the co-moving frame of the growth layer in an expanding colony. Nutrients are supplied from both the top and bottom of the chamber by diffusion so that all cells grow at the same rate (Fig. S4). Cells out of the growth layer are flushed away by continuous medium flow. (c) Proportion of color-switched cells whose final clone size is greater than n, where area is used as a proxy for clone size. The different lines indicate experimental replicas with respectively 45 (blue), 64 (green), 150 (red), 245 (cyan) mutant clones. (d) Relationship between final clone size and distance from the front at which such clone arose. Colors are as in panel (c). The black line corresponds to λ/Δ, where λ is the size of the chamber and Δ is the distance from the front.

During the course of the experiment, we observed both surfing clones, which are born at the very front, as well as non-surfing clones, which are born behind the front (Fig. 3b). Although the occurrence of surfing events is rare, they generate very large clones ($10^2 - 10^3$ cells each) by staying at the front for a while, showing qualitatively different dynamics from the non-surfing clones, in agreement with our simulations (Fig. 2b).

Using clone area as a proxy for size, we obtained the clone size distribution by tracking non-surfing clones for 19-50 hours. The resulting distribution exhibits a power-law decay in agreement with our simulations and theory (Fig. 3c). The relationship between position at birth and final clone size, reported in Fig. 3d, is also consistent with the theoretical prediction for uniform growth within the growth layer. This experiment shows the robustness of our prediction in spite of the complexity of a real cellular population such as cell death, aging of mothers, or feedback of mechanical pressures on growth rate.

2.3. Reconstruction of clone size distribution from subsamples

By characterizing the behavior of the low-frequency mutations, the complete picture of the clone size distribution in crowded expanding populations can now be assessed over the whole frequency range. The full distribution (black line in Fig. 4) exhibits three distinct regimes: non-surfing clones at low frequencies, surfing bubbles at intermediate frequencies and surfing sectors at high frequencies (grey shades in Fig. 4). Using population sequencing, one can capture the complete distribution only by sequencing unrealistically deeply (over 10^5X coverage). With a typical coverage (10 or 100X), population sequencing is likely able to assess only the high frequency regimes [33] (red line in Fig. 4a), and miss the non-surfing bubble behavior that accounts for most of the genetic diversity. However, other sampling strategies can be chosen to take advantage of the spatial proximity of cells that are closely related, practice that is becoming increasingly frequent in cancer research [52, 53, 54, 55, 36, 37, 56]. We find that sampling all the cells in a small contiguous region of the colony is capable of detecting non-surfing clones and the transition between non-surfing and surfing clones (magenta and cyan line in Fig. 4a). The data from these contiguous regions can be appropriately rescaled (Fig. 4b, see Methods for rescaling details) in order to recover the complete behavior of the clone size distribution. The local spatial distribution of mutations can therefore be used to identify non-homogeneous growth in the population by sequencing well-chosen sub-samples.

Discussion

A single resistant cell can suffice to seed an entirely resistant new population in the wake of an antibiotic attack. To predict the chances of success of a drug therapy, it is therefore crucial to assess not just the high frequency mutations carried by a large part of the population, but also the rare ones present in few individuals. In well-mixed populations, the probability distribution of a mutation carried by at least a frequency x is $1/x$ across the frequency range. Allele surfing, a hallmark of spatial growth, has been shown to give rise to a different probability distribution characterized by an excess of mutational jackpot events [33]. Here, we have shown that, while this simple model can explain the behavior of large clones, it fails to describe the majority of mutations which

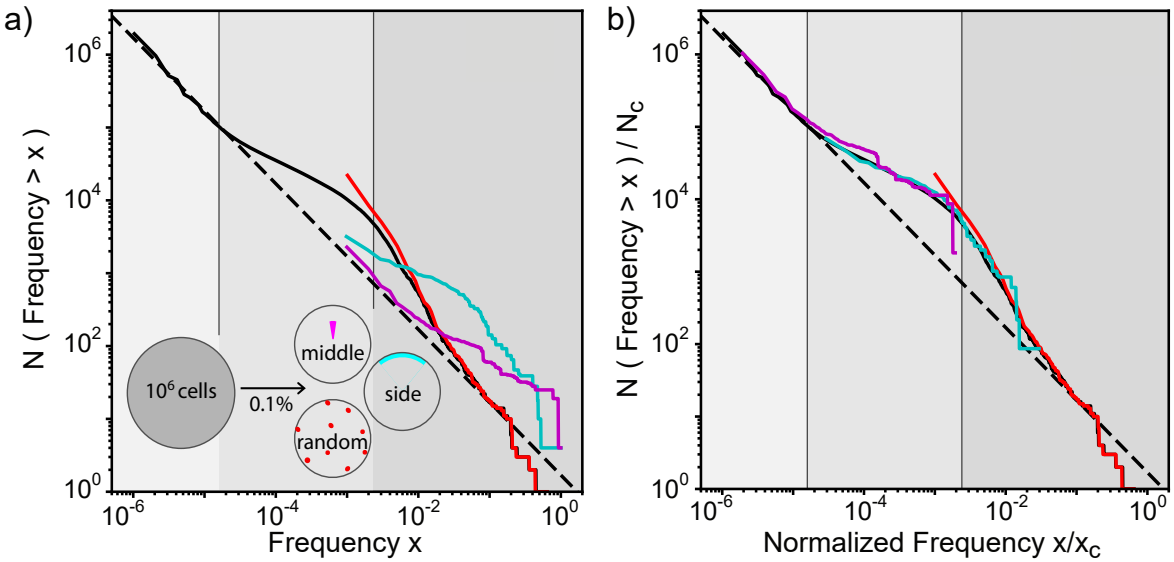

Figure 4. Results from multiple sampling strategies can be combined to infer mutation rate and growth dynamic of the population. (a) Different sampling methods generate distinct clone size distributions that highlight distinct properties of the growth dynamics. This in stark contrast with well-mixed populations where the sampling scheme does not affect the clone size distribution (only lowest detectable frequency). The black solid line represents the clone size distribution of the whole simulated colony (growth layer $\lambda = 14$ cells) grown up to 10^6 cells. We identify three frequency x ranges in the site frequency spectrum: (i) for $x < \lambda/N$, the distribution is dominated by non-surfing clones; (ii) for $\lambda/N < x < 0.01$, allele surfing dominates generating bubbles and sectors as previously described; (iii) for $x > 0.01$, we see a third behavior, generated by mutations that arise in the first few generations, when the whole microcolony is growing exponentially ($N < \pi\lambda^2$). The grayscale regions correspond to non-surfing bubbles (light gray), surfing bubbles (intermediate gray), and sectors (darkest gray). Sampling 0.1 % of the population (equivalent to a 1000X coverage in sequencing) can target non-surfing small clones and generate their corresponding distribution (middle, magenta), or high-frequency surfing clones (random, red). Sampling an outer segment generates a shifted distribution where distinct trends can be observed. (b) These sampling techniques can be combined to reproduce the entire clone size distribution. The rescaling used here requires only knowledge of the total number of cells in the colony and the size/shape of the sampled region, as are described in SI Section 8.

reach much lower frequencies.

Crowded growth in dense populations leads to clones whose final size is determined not by *when*, but rather by *where* the corresponding mutation first arose relative to the expanding front. Large surfing clones, which are well-described by the surface growth properties of the population, must arise at the very front of the expanding edge [57]. Most mutations, however, occur just behind the front, within the growth layer. The final clone size for mutations occurring behind the front is dictated by the mutant cells starting positions, as they are pushed out of the growth layer by the proliferating cells in front due of volume-exclusion effects. This process leads to a reproducible relationship between final clone size and initial position of the first mutant cell, which generates a

clone size distribution different from that of surfing clones.

Because clone size is only determined by the relative position to the front, our argument to derive the full distribution is not limited to two-dimensional colonies expanding at the outer edge, but can be applied to a wider class of populations. Interestingly, further theoretical analysis reveals that the results hold in any system where (i) growth rate varies only along the direction of expansion, (ii) a reference frame can be defined in which the growth profile is constant over time, and (iii) the mutation rate per generation is proportional to the net growth rate (see SI). Under these conditions, the clone size distribution describing small clones decays like x^{-1} up to a critical size that depends only on the growth layer depth but is independent of the number of dimensions (circular colonies vs. solid tumors, see SI), origin of growth (outer vs. inner growth, see SI) or mode of proliferation (budding vs. symmetric division, see SI), showing the robustness of the distribution. These theoretical predictions can be potentially tested with our microfluidic model system, utilizing a tunable switching rate and spatial gradient of nutrients (Fig. S3, S4).

If mutation rate and net growth rate are not proportional, as for instance might be the case in the presence of a non-homogeneous death rate, we find that while the relationship between position at birth and final clone size holds, the clone size distribution deviates from the x^{-1} decay in a way that depends on the ratio between the net growth rate and the mutation rate (see SI for examples).

As the population expands, the majority of mutations are left behind in the bulk, forming a reservoir of genetic diversity in the population. In a typical microbial colony with a growth layer of approximately 100 cells, these mutations would account for more than 99 % of the genetic diversity. Analogously, in a solid tumor, they would be responsible for the vast majority of the intra-tumor heterogeneity, while being largely undetectable by population sequencing. As this class of mutations is the most abundant, it is likely to harbor those rare mutations that can confer resistance. Upon environmental changes that kill the surrounding wild-type, these mutants can be spatially released and thus rescue the population from extinction [33, 58]. It is therefore crucial to develop methodologies that enable their detection.

In well-mixed populations, the detection power is limited by the sequencing coverage one can afford. Still, because the clone size distribution is characterized by a single process across the full range of frequencies, it is possible to estimate mutation rates and selection effects using a reasonable depth of sequencing. Here we have shown that this procedure cannot be applied to crowded populations growing in space, since the shape of the clone size distribution is controlled by very different processes at low and high frequencies. A way around this problem consists in exploiting the spatial arrangement of the population. Neighboring cells are likely to be more closely related than cells farther apart, therefore concentrating sampling power to one location in the population would allow to reach deeper into the low-frequency regime and measure important population genetic parameters like the mutation rate.

In the context of cancer, where there are active debates on how to distinguish

selection from neutral evolution [59, 60], our findings highlight the additional challenge of distinguishing selection effects from non-uniform growth that is exclusively driven by spatial constraints. Here we offer a strategy to identify the specific signatures that crowded growth leaves in the clone size distribution of a population by employing different sampling protocols. These results can help better characterize the growth dynamics of the tumor, which should be used to choose an appropriate null model to identify signatures of selection.

3. Methods

3.1. Fluctuation test in E. coli

The mutator strain *mutT* of the bacterium *E. coli* was used for the fluctuation test experiment on nalidixic acid. The spontaneous mutation rate in this strain was estimated to be approximately $2 \cdot 10^{-7}$ per generation. Colonies starting from single cells were grown on plates with LB and 2 % agar at 37 °C for 30 hours up to a population size between 10^8 and $5 \cdot 10^8$ cells. Each of the 234 colonies was completely scooped from the plate with a pipette tip and resuspended in PBS. A 100X dilution of the resuspension was stored in the fridge for further analysis, while the rest was plated on selective plates containing LB, 2 % agar and 30 μg/mL of nalidixic acid for CFU count. The selective plates were incubated overnight at 37 °C and imaged the following day. CFU count was determined semi-manually with a built-in ImageJ function (see below). If selective plates exhibited more than 400 CFUs, the set-aside 100X dilution was itself plated on nalidixic acid, incubated overnight, and imaged the following day to better estimate the size of large mutations. In the control experiment under well-mixed condition, populations were started from about 50 cells in 200 μL of LB and incubated on a table-top shaker overnight up to saturation. The final population size was estimated to be between 10^8 and 10^9. Each of the 178 well-mixed populations was treated similarly as described above.

3.2. Colony counting on plates

Images of colonies on plates were thresholded and binarized using ImageJ. Thresholding was done manually for each image to minimize the effect of noise, such as dust particles, smudges, or glares. Colonies near the rim of the plates were excluded to avoid an edge effect. Colony counting was done automatically with the Analyze particles function of ImageJ. The final clone size of the well-mixed populations control was rescaled by 10 to take into account the different final population size and to better visualize the comparison with the data from colonies.

3.3. Mechanical simulations

Cells are modeled as 2D rigidly-attached disks that proliferate via budding. Upon division, cells divide in polarly, with newly-formed buds retaining the orientation of their

mothers. Cells interact with each other upon contact via purely repulsive elastic forces and move via overdamped Stokesian dynamics [31]. To mimic diffusion of nutrients into the population from the exterior, we allow only cells within a distance λ from the front to actively grow while the rest of the population remains in stationary phase. In order to simulate a flat geometry, we impose periodic boundary conditions in the horizontal direction so that the populations expands outward only in the vertical direction. To calculate the frequency of neutral mutations, we periodically label $40,000$ newly-born cells and track their descendants.

3.4. Fabrication of microfluidics

The microfluidics was fabricated by soft lithography [61]. The master mold was made by spin-coating (CEE 100 spin coater, Brewer Science) a 10μm-thick layer of negative photoresist (SU8-2010, MicroChem) on a silicon wafer (WaferNet). The photoresist was patterned by photolithography on a mask aligner (Hybralign 200, OAI) through a chrome photomask (Compugraphics). The thickness of the pattern was measured by a stylus meter (Dektak3030, Bruker). Polydimethylsiloxane (PDMS, Sylgard 184, Dow Corning) was mixed with the crosslinker in 10-to-1 ratio and poured on the mold. After being cured at 60 °C overnight, the PDMS was peeled off from the mold and punched holes in for inlets and outlets. The chip was bonded to a glass coverslip after O_2 plasma treatment by a reactive ion etcher (Plasma Equipment Technical Services). Prior to cell culture, 0.1 % bovine serum albumin (Sigma-Aldrich) was loaded into the device to reduce the interaction between cells and the substrate.

3.5. Yeast Strain

The microfluidics experiments were conducted with the *S. cerevisiae* strain yJK10, derived from strain yDM117 (courtesy of Jasper Rine, University of California, Berkeley). yJK10 employs a Cre-loxP recombination system to switch stochastically from a red (yEmRFP) to a green (yEGFP) fluorescent state, as previously published [33, 40]. Using an estradiol-inducible Cre construct allowed us to optimize the average switching rate for our experiments[62]. For all experiments we used a concentration of 1.6 nM β-estradiol corresponding to a switching rate of $7.1 \pm 4.8 \times 10^{-4}$ per cell per generation (estimated from the number of observed switching during the microfluidics experiments). In principle, the relative fitness between switched and unswitched cells can be set via the differing cycloheximide susceptibility of both states. However, while we did not perform any variation of relative fitness in this study, we chose to use yJK10 to maximize comparability of our results to ongoing and future investigations involving this strain. Under our experimental condition, the relative fitness between the two states ($s = 0.022 \pm 0.040$) is sufficiently small to be neglected (Fig. S5). See the SI for the effect of non-zero s on the power-law exponent of the distribution of clone size.

3.6. Clone tracking in microfluidics

The microfluidic growth chamber was designed as a population version of the mother machine [39]. A suspension of yJK10 cells in an exponential phase was injected into the device with YPD culture medium. After overnight culture, cells grew and filled up the growth chamber. At this point, 1.6 nM β-estradiol was added to the culture medium to induce color switching (the switching rate was about 10^{-3} per cell division). Subsequent growth was imaged using time-lapse microscopy on an inverted microscope (IX81, Olympus) with a 10X objective every 10 minutes for 2-4 days. The taken GFP images (color of switched cells) were binarized by Otsus method [63], and the dynamics of the clones were manually tracked on Matlab (Mathworks) and ImageJ (NIH). Throughout the experiment, the temperature was controlled at 30 °C by a microscope incubator (H201-T, Okolab), and the flow rate of the medium was regulated by syringe pumps (neMESYS, CETONI) at 15 μL/h. The growth rate of cells was uniform across the chamber under our experimental condition (Fig. S4) [64].

Data availability

All data, codes, scripts and CAD files for microfluidics are available upon request.

Acknowledgement

References

[1] C. D. Nadell, K. Drescher, and K. R. Foster, "Spatial structure, cooperation and competition in biofilms," *Nature Reviews Microbiology*, vol. 14, no. 9, p. 589, 2016.

[2] C. J. Chan, C.-P. Heisenberg, and T. Hiiragi, "Coordination of morphogenesis and cell-fate specification in development," *Current Biology*, vol. 27, no. 18, pp. R1024–R1035, 2017.

[3] B. Waclaw, I. Bozic, M. E. Pittman, R. H. Hruban, B. Vogelstein, and M. A. Nowak, "A spatial model predicts that dispersal and cell turnover limit intratumour heterogeneity," *Nature*, vol. 525, no. 7568, p. 261, 2015.

[4] C. Carmona-Fontaine, M. Deforet, L. Akkari, C. B. Thompson, J. A. Joyce, and J. B. Xavier, "Metabolic origins of spatial organization in the tumor microenvironment," *Proceedings of the National Academy of Sciences*, vol. 114, no. 11, pp. 2934–2939, 2017.

[5] K. J. Lenos, D. M. Miedema, S. C. Lodestijn, L. E. Nijman, T. van den Bosch, X. R. Ros, F. C. Lourenço, M. C. Lecca, M. van der Heijden, S. M. van Neerven, *et al.*, "Stem cell functionality is microenvironmentally defined during tumour expansion and therapy response in colon cancer," *Nature cell biology*, vol. 20, no. 10, p. 1193, 2018.

[6] M. van der Heijden, D. M. Miedema, B. Waclaw, V. L. Veenstra, M. C. Lecca, L. E. Nijman, E. van Dijk, S. M. van Neerven, S. C. Lodestijn, K. J. Lenos, *et al.*, "Spatiotemporal regulation of clonogenicity in colorectal cancer xenografts," *Proceedings of the National Academy of Sciences*, vol. 116, no. 13, pp. 6140–6145, 2019.

[7] L. Vermeulen, E. Morrissey, M. van der Heijden, A. M. Nicholson, A. Sottoriva, S. Buczacki, R. Kemp, S. Tavare, and D. J. Winton, "Defining stem cell dynamics in models of intestinal tumor initiation," *Science*, vol. 342, no. 6161, pp. 995–998, 2013.

[8] A. M. Klein and B. D. Simons, "Universal patterns of stem cell fate in cycling adult tissues," *Development*, vol. 138, no. 15, pp. 3103–3111, 2011.

[9] S. Rulands and B. D. Simons, "Tracing cellular dynamics in tissue development, maintenance and disease," *Current Opinion in Cell Biology*, vol. 43, pp. 38–45, 2016.

[10] S. Chabab, F. Lescroart, S. Rulands, N. Mathiah, B. D. Simons, and C. Blanpain, "Uncovering the Number and Clonal Dynamics of Mesp1 Progenitors during Heart Morphogenesis," *Cell Reports*, vol. 14, no. 1, pp. 1–10, 2016.

[11] C. Carmona-Fontaine, V. Bucci, L. Akkari, M. Deforet, J. A. Joyce, and J. B. Xavier, "Emergence of spatial structure in the tumor microenvironment due to the Warburg effect," *Proceedings of the National Academy of Sciences*, vol. 110, no. 48, pp. 19402–19407, 2013.

[12] S. Lamprecht, E. M. Schmidt, C. Blaj, H. Hermeking, A. Jung, T. Kirchner, and D. Horst, "Multicolor lineage tracing reveals clonal architecture and dynamics in colon cancer," *Nature Communications*, vol. 8, no. 1, pp. 1–8, 2017.

[13] V. D. Varner, J. P. Gleghorn, E. Miller, D. C. Radisky, and C. M. Nelson, "Mechanically patterning the embryonic airway epithelium," *Proceedings of the National Academy of Sciences*, vol. 112, no. 30, pp. 9230–9235, 2015.

[14] M. D. Ryser, B.-H. Min, K. D. Siegmund, and D. Shibata, "Spatial mutation patterns as markers of early colorectal tumor cell mobility," *Proceedings of the National Academy of Sciences*, vol. 115, no. 22, pp. 5774–5779, 2018.

[15] M. Baym, T. D. Lieberman, E. D. Kelsic, R. Chait, R. Gross, I. Yelin, and R. Kishony, "Spatiotemporal microbial evolution on antibiotic landscapes," *Science*, vol. 353, no. 6304, pp. 1147–1151, 2016.

[16] M. A. Nowak, F. Michor, and Y. Iwasa, "The linear process of somatic evolution," *Proceedings of the National Academy of Sciences*, vol. 100, no. 25, pp. 14966–14969, 2003.

[17] F. Michor, Y. Iwasa, H. Rajagopalan, C. Lengauer, and M. A. Nowak, "Linear model of colon cancer initiation," *Cell Cycle*, vol. 3, no. 3, pp. 356–360, 2004.

[18] M. O. Lavrentovich, M. E. Wahl, D. R. Nelson, and A. W. Murray, "Spatially Constrained Growth Enhances Conversional Meltdown," *Biophysical Journal*, vol. 110, no. 12, pp. 2800–2808, 2016.

[19] O. Hallatschek, P. Hersen, S. Ramanathan, and D. R. Nelson, "Genetic drift at expanding frontiers promotes gene segregation," *Proceedings of the National Academy of Sciences*, vol. 104, no. 50, pp. 19926–19930, 2007.

[20] Z. Ahmed and S. Gravel, "Intratumor heterogeneity and circulating tumor cell clusters," *Molecular biology and evolution*, vol. 35, no. 9, pp. 2135–2144, 2017.

[21] H. Tanaka, Z. Zeravcic, and M. P. Brenner, "Mutation at Expanding Front of Self-Replicating Colloidal Clusters," *Physical Review Letters*, vol. 117, no. 23, pp. 1–5, 2016.

[22] S. Peischl, I. Dupanloup, M. Kirkpatrick, and L. Excoffier, "On the accumulation of deleterious mutations during range expansions," *Molecular Ecology*, vol. 22, no. 24, pp. 5972–5982, 2013.

[23] S. Peischl, I. Dupanloup, L. Bosshard, and L. Excoffier, "Genetic surfing in human populations: from genes to genomes," *Current Opinion in Genetics and Development*, vol. 41, pp. 53–61, 2016.

[24] R. Zöllner, E. R. Oldewurtel, N. Kouzel, and B. Maier, "Phase and antigenic variation govern competition dynamics through positioning in bacterial colonies," *Scientific Reports*, vol. 7, no. 1, pp. 1–12, 2017.

[25] C. C. Traverse, L. M. Mayo-Smith, S. R. Poltak, and V. S. Cooper, "Tangled bank of experimentally evolved Burkholderia biofilms reflects selection during chronic infections," *Proceedings of the National Academy of Sciences*, vol. 110, no. 3, pp. E250–E259, 2013.

[26] F. D. Farrell, M. Gralka, O. Hallatschek, and B. Waclaw, "Mechanical interactions in bacterial colonies and the surfing probability of beneficial mutations," *Journal of The Royal Society Interface*, vol. 14, no. 131, p. 20170073, 2017.

[27] M. O. Lavrentovich, J. H. Koschwanez, and D. R. Nelson, "Nutrient shielding in clusters of cells," *Physical Review E*, vol. 87, no. 6, p. 062703, 2013.

[28] J.-R. Meunier and M. Choder, "Saccharomyces cerevisiae colony growth and ageing: biphasic growth accompanied by changes in gene expression," *Yeast*, vol. 15, no. 12, pp. 1159–1169, 1999.

[29] L. Váchová and Z. Palková, "How structured yeast multicellular communities live, age and die?," *FEMS yeast research*, vol. 18, no. 4, p. foy033, 2018.

[30] S. Pirt, "A kinetic study of the mode of growth of surface colonies of bacteria and fungi," *Microbiology*, vol. 47, no. 2, pp. 181–197, 1967.

[31] J. Kayser, C. F. Schreck, M. Gralka, D. Fusco, and O. Hallatschek, "Collective motion conceals fitness differences in crowded cellular populations," *Nature Ecology & Evolution*, vol. 3, p. 125, 2019.

[32] A. Giometto, D. R. Nelson, and A. W. Murray, "Physical interactions reduce the power of natural selection in growing yeast colonies," *Proceedings of the National Academy of Sciences*, vol. 115, no. 45, pp. 11448–11453, 2018.

[33] D. Fusco, M. Gralka, J. Kayser, A. Anderson, and O. Hallatschek, "Excess of mutational jackpot events in expanding populations revealed by spatial Luria-Delbrück experiments," *Nature Communications*, vol. 7, p. 12760, 2016.

[34] L. Excoffier and N. Ray, "Surfing during population expansions promotes genetic revolutions and structuration," *Trends in ecology & evolution*, vol. 23, no. 7, pp. 347–351, 2008.

[35] U. D. Monte, "Does the cell number 109 still really fit one gram of tumor tissue?," *Cell Cycle*, vol. 8, no. 3, pp. 505–506, 2009. PMID: 19176997.

[36] A. Sottoriva, H. Kang, Z. Ma, T. A. Graham, M. P. Salomon, J. Zhao, P. Marjoram, K. Siegmund, M. F. Press, D. Shibata, *et al.*, "A big bang model of human colorectal tumor growth," *Nature genetics*, vol. 47, no. 3, p. 209, 2015.

[37] M. J. Williams, B. Werner, C. P. Barnes, T. A. Graham, and A. Sottoriva, "Identification of neutral tumor evolution across cancer types," *Nature genetics*, vol. 48, no. 3, p. 238, 2016.

[38] S. Luria and M. Delbrück, "Mutations of Bacteria from Virus Sensitivity to Virus Resistance.," *Genetics*, vol. 28, no. 6, pp. 491–511, 1943.

[39] P. Wang, L. Robert, J. Pelletier, W. L. Dang, F. Taddei, A. Wright, and S. Jun, "Robust growth of escherichia coli," *Current Biology*, vol. 20, no. 12, pp. 1099–1103, 2010.

[40] A. E. Dodson and J. Rine, "Heritable capture of heterochromatin dynamics in saccharomyces cerevisiae," *Elife*, vol. 4, p. e05007, 2015.

[41] H. B. Newcombe, "Origin of bacterial variants," *Nature*, vol. 164, no. 4160, p. 150, 1949.

[42] K. C. Atwood, L. K. Schneider, and F. J. Ryan, "Periodic selection in escherichia coli," *Proceedings of the National Academy of Sciences*, vol. 37, no. 3, pp. 146–155, 1951.

[43] J. Lederberg and E. M. Lederberg, "Replica plating and indirect selection of bacterial mutants," *Journal of Bacteriology*, vol. 63, no. 3, p. 399, 1952.

[44] B. J. Thomas and R. Rothstein, "Elevated recombination rates in transcriptionally active dna," *Cell*, vol. 56, no. 4, pp. 619–630, 1989.

[45] C. F. Pope, D. M. O'Sullivan, T. D. McHugh, and S. H. Gillespie, "A practical guide to measuring mutation rates in antibiotic resistance," *Antimicrobial agents and chemotherapy*, vol. 52, no. 4, pp. 1209–1214, 2008.

[46] D. E. Lea and C. A. Coulson, "The distribution of the numbers of mutants in bacterial populations," *Journal of Genetics*, vol. 49, no. 3, pp. 264–285, 1949.

[47] M. Delarue, J. Hartung, C. Schreck, P. Gniewek, L. Hu, S. Herminghaus, and O. Hallatschek, "Self-driven jamming in growing microbialpopulations," *Nature Physics*, vol. 12, p. 762, 2016.

[48] W. Mather, O. Mondragón-Palomino, T. Danino, J. Hasty, and L. S. Tsimring, "Streaming instability in growing cell populations," *Physical review letters*, vol. 104, no. 20, p. 208101, 2010.

[49] D. Boyer, W. Mather, O. Mondragón-Palomino, S. Orozco-Fuentes, T. Danino, J. Hasty, and L. S. Tsimring, "Buckling instability in ordered bacterial colonies," *Physical biology*, vol. 8, no. 2, p. 026008, 2011.

[50] G. Lambert and E. Kussell, "Memory and fitness optimization of bacteria under fluctuating environments," *PLoS genetics*, vol. 10, no. 9, p. e1004556, 2014.

[51] W.-H. Lin and E. Kussell, "Complex interplay of physiology and selection in the emergence of

antibiotic resistance," *Current Biology*, vol. 26, no. 11, pp. 1486–1493, 2016.

[52] M. Gerlinger, A. J. Rowan, S. Horswell, J. Larkin, D. Endesfelder, E. Gronroos, P. Martinez, N. Matthews, A. Stewart, P. Tarpey, *et al.*, "Intratumor heterogeneity and branched evolution revealed by multiregion sequencing," *New England journal of medicine*, vol. 366, no. 10, pp. 883–892, 2012.

[53] E. C. de Bruin, N. McGranahan, R. Mitter, M. Salm, D. C. Wedge, L. Yates, M. Jamal-Hanjani, S. Shafi, N. Murugaesu, A. J. Rowan, *et al.*, "Spatial and temporal diversity in genomic instability processes defines lung cancer evolution," *Science*, vol. 346, no. 6206, pp. 251–256, 2014.

[54] J. Zhang, J. Fujimoto, J. Zhang, D. C. Wedge, X. Song, J. Zhang, S. Seth, C.-W. Chow, Y. Cao, C. Gumbs, *et al.*, "Intratumor heterogeneity in localized lung adenocarcinomas delineated by multiregion sequencing," *Science*, vol. 346, no. 6206, pp. 256–259, 2014.

[55] S. Ling, Z. Hu, Z. Yang, F. Yang, Y. Li, P. Lin, K. Chen, L. Dong, L. Cao, Y. Tao, *et al.*, "Extremely high genetic diversity in a single tumor points to prevalence of non-darwinian cell evolution," *Proceedings of the National Academy of Sciences*, vol. 112, no. 47, pp. E6496–E6505, 2015.

[56] R. Sun, Z. Hu, A. Sottoriva, T. A. Graham, A. Harpak, Z. Ma, J. M. Fischer, D. Shibata, and C. Curtis, "Between-region genetic divergence reflects the mode and tempo of tumor evolution," *Nature genetics*, vol. 49, no. 7, p. 1015, 2017.

[57] M. Gralka, F. Stiewe, F. Farrell, W. Möbius, B. Waclaw, and O. Hallatschek, "Allele surfing promotes microbial adaptation from standing variation," *Ecology letters*, vol. 19, no. 8, pp. 889–898, 2016.

[58] J. Gallaher, P. M. Enriquez-Navas, K. A. Luddy, R. A. Gatenby, and A. R. Anderson, "Spatial heterogeneity and evolutionary dynamics modulate time to recurrence in continuous and adaptive cancer therapies," *Cancer research*, pp. canres–2649, 2018.

[59] M. Tarabichi, I. Martincorena, M. Gerstung, A. M. Leroi, F. Markowetz, S. C. Dentro, I. Leshchiner, M. Gerstung, C. Jolly, K. Haase, M. Tarabichi, J. Wintersinger, A. G. Deshwar, K. Yu, S. Gonzalez, Y. Rubanova, G. Macintyre, D. J. Adams, P. Anur, R. Beroukhim, P. C. Boutros, D. D. Bowtell, P. J. Campbell, S. Cao, E. L. Christie, M. Cmero, Y. Cun, K. J. Dawson, J. Demeulemeester, N. Donmez, R. M. Drews, R. Eils, Y. Fan, M. Fittall, D. W. Garsed, G. Getz, G. Ha, M. Imielinski, L. Jerman, Y. Ji, K. Kleinheinz, J. Lee, H. Lee-Six, D. G. Livitz, S. Malikic, F. Markowetz, I. Martincorena, T. J. Mitchell, V. Mustonen, L. Oesper, M. Peifer, M. Peto, B. J. Raphael, D. Rosebrock, S. C. Sahinalp, A. Salcedo, M. Schlesner, S. Schumacher, S. Sengupta, R. Shi, S. J. Shin, L. D. Stein, I. Vázquez-García, S. Vembu, D. A. Wheeler, T.-P. Yang, X. Yao, K. Yuan, H. Zhu, W. Wang, Q. D. Morris, P. T. Spellman, D. C. Wedge, P. Van Loo, P. T. Spellman, Q. D. Morris, O. C. Lingjærde, D. C. Wedge, P. Van Loo, T. P. E. Group, and H. Working, "Neutral tumor evolution?," *Nature Genetics*, vol. 50, no. 12, pp. 1630–1633, 2018.

[60] T. Heide, L. Zapata, M. J. Williams, B. Werner, G. Caravagna, C. P. Barnes, T. A. Graham, and A. Sottoriva, "Reply to a 'Neutral tumor evolution?'," *Nature Genetics*, vol. 50, no. 12, pp. 1633–1637, 2018.

[61] J. C. McDonald, D. C. Duffy, J. R. Anderson, D. T. Chiu, H. Wu, O. J. Schueller, and G. M. Whitesides, "Fabrication of microfluidic systems in poly(dimethylsiloxane).," *Electrophoresis*, vol. 21, no. 1, pp. 27–40, 2000.

[62] D. L. Lindstrom and D. E. Gottschling, "The mother enrichment program: A genetic system for facile replicative life span analysis in Saccharomyces cerevisiae," *Genetics*, 2009.

[63] N. Otsu, "A Threshold Selection Method from Gray-Level Histograms," *IEEE Transactions on Systems, Man, and Cybernetics*, vol. 9, no. 1, pp. 62–66, 1979.

[64] W. Thielicke and E. J. Stamhuis, "Pivlab-towards user-friendly, affordable and accurate digital particle image velocimetry in matlab," *Journal of Open Research Software*, vol. 2, no. 1, p. e30, 2014.